# Supramolecular Nanostructures as Support Materials for Gold Nanoparticle Catalysts

by

Kiera Y. Tai

Submitted to the Department of Materials Science and Engineering
in partial fulfillment of the requirements for the degree of

Bachelor of Science in Materials Science and Engineering

at the

MASSACHUSETTS INSTITUTE OF TECHNOLOGY

May 2022



Author .....
Department of Materials Science and Engineering
May 06, 2022

Certified by .....
Julia Ortony
Samuel A. Goldblith Assistant Professor in Materials Science and Engineering
Thesis Supervisor

Accepted by .....
James LeBeau
John Chipman Associate Professor of Materials Science and Engineering
Chair, DMSE Undergraduate Committee

# Supramolecular Nanostructures as Support Materials for Gold Nanoparticle Catalysts

by

Kiera Y. Tai

Submitted to the Department of Materials Science and Engineering
on May 06, 2022, in partial fulfillment of the
requirements for the degree of
Bachelor of Science in Materials Science and Engineering

## Abstract

The high catalytic activity of gold nanoparticles (AuNPs) has led to their use in a variety of industrially-relevant reactions, such as low-temperature CO-oxidation and selective alcohol oxidation. Most current research focuses on heterogenous gold catalysis, with metal oxides being the most commonly employed support material for AuNPs. However, metal oxides are challenging to evenly distribute in solution and intrinsically difficult to modify. Molecular self-assembly provides a novel route to synthesize AuNP support materials, offering precise control over spatial arrangements and tunable surface chemistries. A particularly promising self-assembled molecule is the aramid amphiphile (AA), which overcomes the typical mechanical fragility of self-assembled structures by incorporating a Kevlar-inspired domain into its molecular structure. In this work, we present a cysteine-functionalized aramid amphiphile platform (CysAA) for AuNP stabilization, which exhibits favorable surface chemical affinity to gold. We show that AuNPs are anchored on the surface of CysAA which can be evenly dispersed in solution, enabling quasi-homogeneous catalysis in aqueous conditions. Furthermore, the high aspect-ratio of these nanostructures allows for the recovery and recycling of AuNPs from solution by simple filtration. Using the model reduction reaction of 4-nitrophenol, we demonstrate the catalytic activity and recyclability of this AuNP-CysAA catalyst.

Thesis Supervisor: Julia Ortony
Title: Samuel A. Goldblith Assistant Professor in Materials Science and Engineering

# Acknowledgments

First and foremost, I would like to thank my thesis advisor Professor Julia Ortony and my project supervisor Yukio Cho for their guidance, patience, and willingness to answer my questions at all hours of the day (and night). I would also like to thank the entirety of the Ortony Lab for making me feel so welcome this past year.

I am very grateful to the Department of Materials Science and Engineering - both my professors and my peers - for an exceptional undergraduate academic experience and such a warm, inviting community.

I must also acknowledge my instructors in the School of Humanities, Arts, and Social Sciences, particularly those in the music and literature departments, that have so uniquely enriched my time here.

To my friends, thank you for sticking with me as we navigated the ups and downs of MIT these past four years. And finally, to my family, thank you for the endless love and support that has kept me warm through the coldest of Boston winters.

# Contents

# List of Figures

# List of Tables

# Chapter 1

# Introduction

## 1.1 Gold in the age of nanotechnology

As a material, gold has captivated humankind since ancient times. Predominantly sought after for its luster, elemental gold was known to be chemically inert for most of history and thus did not attract significant scientific attention. In recent decades, however, the rapidly developing fields of nanoscience and nanotechnology have cast gold under a new light. Applications of gold nanoparticles have become an increasingly active area of research in a variety of fields, including chemistry, biology and pharmacy [1].

Nanoparticles are defined by the American Society for Testing and Materials (ASTM) as particles within the size range of 1-100 nm [2]. Consequentially, nanoparticles have an extremely high surface area to volume ratio, which gives them unique properties that are completely different from their bulk counterparts [1]. These physio-chemical differences become especially clear in the areas of reactivity, toughness, and optics [3].

Nanoparticles can be structurally complex: many are composed of multiple layers including different surface, shell, and core materials. Metal nanoparticles are composed entirely of their constituent metals, though they can be synthesized into various geometries [1]. One of the most immediately striking characteristics of metal nanoparticles is their color; because of their small size, they absorb and reflect dif-

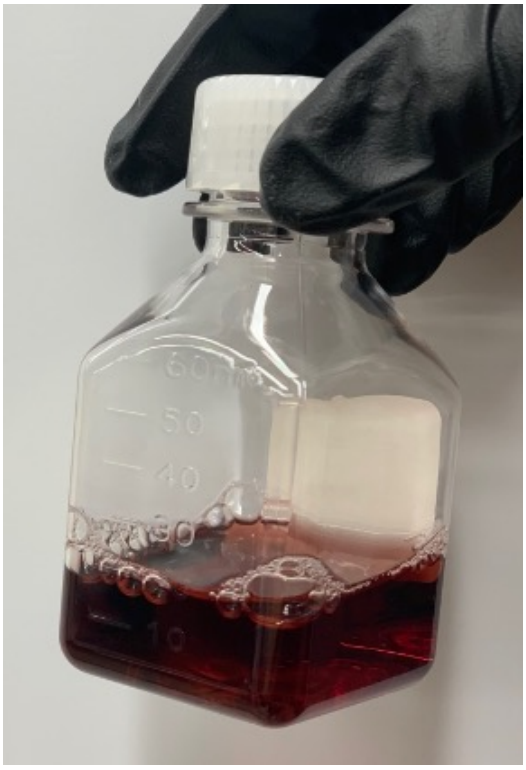

**Figure 1-1:** Colloidal gold nanoparticles.

ferent wavelengths of light than their bulk versions. Gold nanoparticles, for instance, express a wine-red color (Figure 1-1). The shade of red can also vary based on shape, size, and concentration [1].

Gold nanoparticles (AuNPs) are particularly sought after in chemical catalysis and biomedical research. AuNPs are attractive catalysts because they exhibit high chemical reactivity and catalytic activity, even at cold and mild temperatures [4, 5]. In the biomedical sphere, drug delivery is the chief application of AuNPs; therapeutic agents can be conjugated onto AuNP surfaces to be released in response to various biological, chemical, thermal, or photo-chemical stimuli [2, 6].

## 1.2 Gold nanoparticles as catalysts

Catalytic AuNPs have a variety of industrially and environmentally significant applications, including the oxidation of alcohols and alkanes [7]. These reactions are directly related to pollution control, where AuNPs have been shown to be effective

in the oxidation CO and other pollutants such as nitrogen-based malodorous compounds, opening the door for many commercial applications in air quality control [8, 4]. Similarly, in water quality control, AuNPs are emerging as a leading candidate for the hydro-chlorination and chelation of common pollutants [4]. There is also recent research in using AuNPs in fuel cells to catalyze the water-gas shift to produce hydrogen from CO and steam [4].

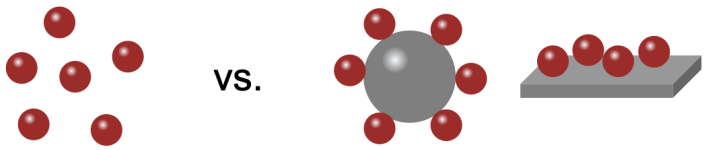


**Figure 1-2:** Schematic of homogeneous AuNP catalysts (left) vs. heterogeneous AuNP catalysts (right). Critically, in the homogenous case, the AuNPs are suspended in solution, while in the heterogeneous case, the AuNPs are anchored onto a solid support material.

Most catalysts can be categorized as either homogeneous or heterogeneous. Homogeneous catalysts exist in the same phase as the reactants, typically gas or solution. Colloidal AuNPs (dispersed in water) fall into this category (Figure 1-2). Homogeneous catalysts are generally effective and selective, but are difficult to separate from the reaction product, limiting their industrial use [9]. Colloidal AuNPs also tend to aggregate, which decreases their reactivity and can case them to precipitate out of solution [10].

On the other hand, heterogeneous catalysts exist in a different phase as the reactants. Metal nanoparticle catalysts are fixated onto a solid support material (usually chemically inert), which helps stabilize the catalyst and facilitates even distribution in solution [11]. AuNP catalysts typically fall in to this category (Figure 1-2). The most common support materials for AuNPs are ceramics such as metal oxides [7, 12]. Typically, these catalysts are synthesized through chemical reduction of a gold precursor (a solution of gold salts) directly onto the metal oxides [5, 7]. While these heterogeneous AuNP catalysts are effective in industrial applications because of their stability and ability to be filtered, there are some drawbacks. In particular, the chem-

ical reduction synthesis approach introduces uncertainty in to the system because it lacks a precise control over the size and geometry of the resulting AuNPs [5, 12]. Furthermore, metal oxides are challenging to disperse evenly in solution and are intrinsically difficult to modify. Since the catalytic activity of AuNPs depend on size and active surface area, optimization of synthesis methods and exploration of novel support materials are active areas of research to enable widespread use of AuNPs [13].

## 1.3 Molecular self-assembly for support materials

In the development of effective and recyclable AuNP support materials, organic small molecules offer a novel and promising solution, chiefly because of their tunability. Generally, catalyst support materials need to have chemical stability, high surface area, and the ability to dispersing metal nanoparticles evenly over its surface [11]. These requirements can be met through targeted organic synthesis approaches.

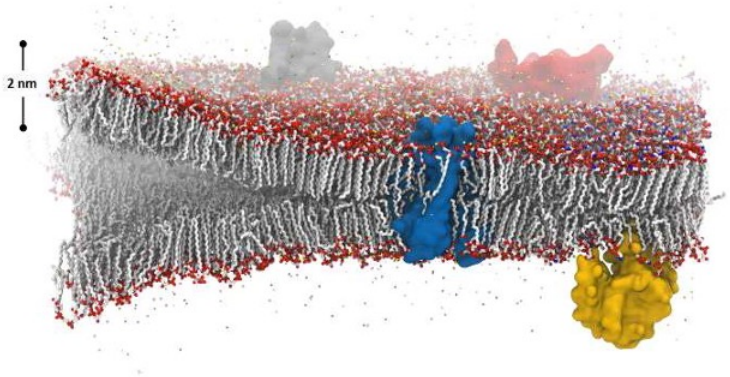


**Figure 1-3:** Schematic of an amphiphilic lipid, formed via spontaneous self-assembly as individual surfactant-like molecules (amphiphiles) arrange to maximize favorable interactions.

We are particularly interested in organic support materials formed via supramolecular assembly, a phenomenon which occurs when small molecules spontaneously form nanostructures. Inspired by the lipid bilayer from biology, these molecules are composed of individual surfactant-like molecules (amphiphiles) that arrange to maximize favorable interactions. In aqueous conditions, self-assembly leverages the hydrophobic

effect (the tendency of water and nonpolar substances to separate) where a hydrophobic species spontaneously self-assembles to minimize surface energy of the resulting nanostructure [14]. This bottom-up design strategy that offers precise spatial arrangement over nanostructures and tunable surface chemistries [15]. In principle, molecular self-assembly can be employed to synthesize a catalyst support material with high surface area and surface affinity to AuNPs.

However, a major drawback of self-assembled nanostructures is that they are generally fragile due to weak intermolecular forces in the aliphatic tail regime. Often, the molecules can move within or between assemblies, leading to the nanostructure's collapse when the driving force is insufficient [16, 17]. Self-assembled structures also typically lose their structural integrity outside of water. This lack of mechanical strength limits their applications in air and thus prevents wide-spread usage. Most current applications of self-assembled molecules are in the biological realm, where the conditions are aqueous and biodegradability is a desirable feature [16, 17].

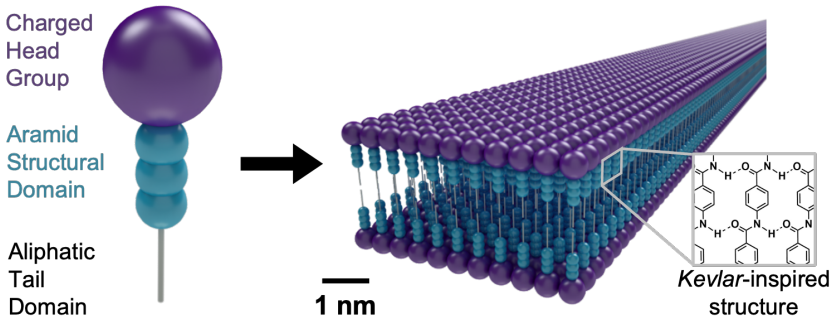


**Figure 1-4:** Schematic of the aramid amphipile, a mechanically robust self-assembled small-molecule platform that incorporates a Kevlar-inspired hydrogen-bonding aramid domain into its molecular structure.

Recent developments, however, have presented a particularly promising self-assembled small-molecule platform: the aramid amphiphile (AA). This nanostructure of the AA overcomes the typical mechanical fragility of self-assembled structures by incorporating a Kevlar-inspired hydrogen-bonding aramid domain into its molecular structure [16]. As a result, AAs exhibits remarkable stability, mechanical robustness, and suppressed dynamic motion. These desirable qualities enable many novel applications,

including the area of AuNP stabilization.

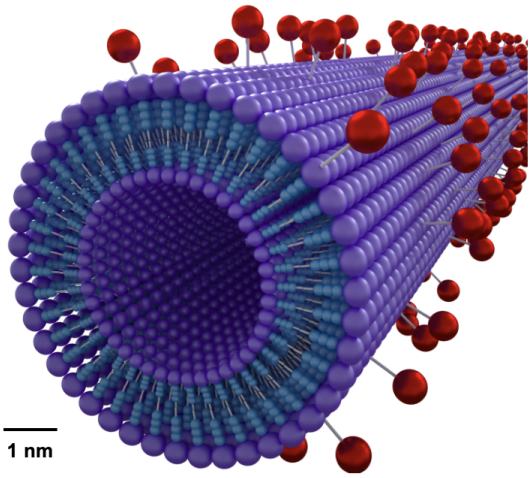


**Figure 1-5:** Schematic of gold nanoparticles binding to the surface of CysAA nanotubes.

By designing the surfaces of AAs with favorable chemical affinity towards gold, this material class could immobilize AuNPs on its surface. In this work, we present a cysteine-functionalized aramid amphiphile platform (CysAA) that forms stable nanotubes in water to be used as AuNP support materials. Specifically, by introducing the sulfur-containing amino acid cysteine as a charged head group onto the aramid amphaphile, we can employ the well-documented gold-thiol bond to bind colloidal AuNPs [18]. With AuNPs anchored on the surface of CysAA, they can can be evenly dispersed in solution, enabling quasi-homogeneous catalysis in aqueous conditions. Furthermore, the high aspect-ratio of these nanostructures allows for the recovery and recycling of AuNPs from solution by simple filtration.

# Chapter 2

# Synthesis of the Cysteine-Functionalized Aramid Amphiphile

## 2.1 Materials

For the synthesis of cysteine-functionalized aramid amphiphiles (CysAA), methyl 4-aminobenzoate (Fisher Chemical, 98%), 3,3-dimethylbutanoic acid (DMBTA, Sigma Aldrich, 98%), 3-(3-Dimethylaminopropyl)-1-ethyl-carbodiimide hydrochloride (EDCI, Chem Impex, ≥99%), 4-Dimethylaminopyridine (DMAP, Chem Impex, ≥99%), sodium bicarbonate ($NaHCO_3$, Thermo Fisher Scientific), lithium hydroxide monohydrate ($LiOH \cdot H_2O$, Thermo Fisher Scientific), hydrochloric acid ($HCl \cdot H_2O$, Fisher Chemical, 36.5 to 38.0%), Boc-4-aminobenzoic acid (Chem Impex, ≥99%), trifluoroacetic acid (TFA, Fisher Chemical, ≥97%), Boc-Cys(Trt)-OH (Sigma Aldrich, 97%), 1-hydroxybenzotriazole hydrate (HOBt, TCI Chemicals, 97%), N,N- Diisopropylethylamine (DIPEA, Alfa Aesar, 99%), and Triisopropylsilane (TIPS, Oakwood Chemicals, 98%) were used as received without further purification.

Solvents used were N,N-Dimethylformamide (DMF, Fisher Chemical, ≥99.8%), methanol (MeOH, Fisher Chemical, ≥99.9%), tetrahydrofuran (THF, Fisher Chem-

ical, ≥99.9%), dichloromethane (DCM, Fisher Chemical, ≥99.6%), and acetonitrile (ACN, Fisher Chemical, ≥99.9%), and de-ionized water.

## 2.2 Synthetic pathway to the aramid structure

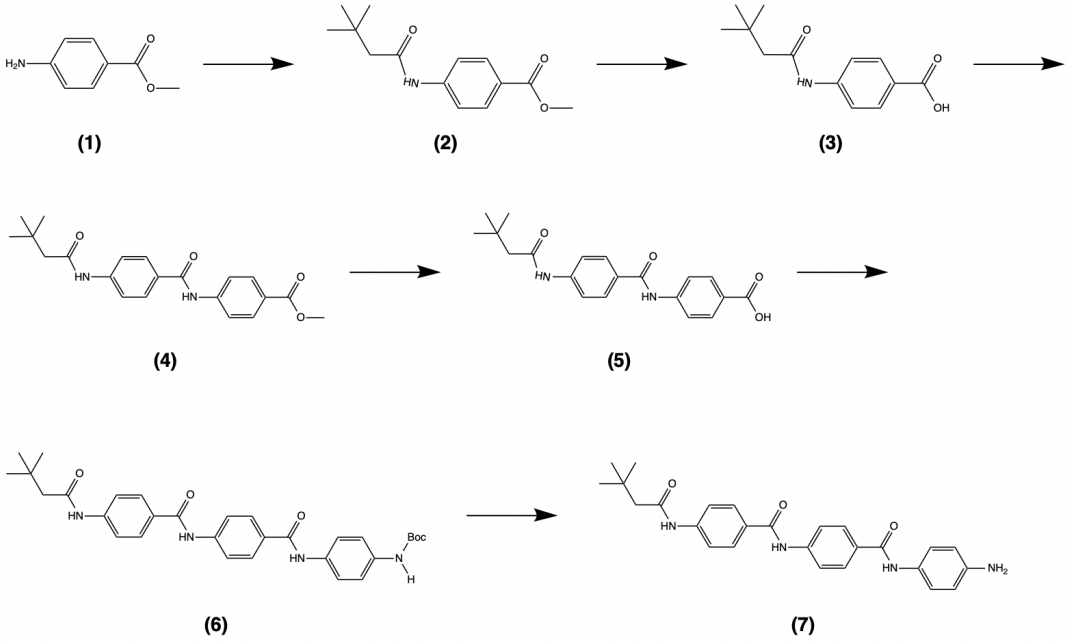


**Figure 2-1:** Synthesis scheme to the aramid structure. Different charged head groups can be attached from this product.

The synthesis of the aramid structure of the aramid amphiphile contained six steps (Figure 2-1). The chemical composition of intermediates and products were confirmed through $^1$H nuclear magnetic resonance (NMR) spectroscopy.

The first step attached the aliphatic tail domain onto a single aramid starting material. Methyl 4-aminobenzoate, DMBTA, EDCI, and DMAP were combined in DMF and mixed at room temperature overnight. The product **(2)** was crashed out in water, collected through vacuum filtration, and washed with MeOH with 5 wt% $NaHCO_3$. (Yield = 73.76%.)

The second step was an ester hydrolysis to create a carboxylic acid end group. The previous product **(2)** (24.46 mmol) was dissolved in a 1:2 ratio of MeOH and THF. LiOH was dissolved in de-ionized water and added to the mixture. The solution was

stirred at 60 °C overnight. The next day, vacuum was used to remove excess solvent and the solid was collected. 1 M HCl was added to the solid until the solution had pH 1. The filtrate **(3)** was collected via vacuum filtration and washed with de-ionized water. (Yield = 100.99%.)

The third step added a second aramid. Methyl 4-aminobenzoate, EDCI, and DMAP were mixed with the previous product **(3)** (24.30 mmol) in DMF and mixed at room temperature overnight. The product **(4)** was crashed out in water, collected through vacuum filtration, and washed with MeOH. (Yield = 87.60%.)

The fourth step was another ester hydrolysis to create a carboxylic acid end group. The previous product **(4)** (19.81 mmol) was dissolved in a 1:2 ratio of MeOH and THF. LiOH was dissolved in de-ionized water and added to the mixture. The solution was stirred at 60 °C overnight. The next day, vacuum was used to remove excess solvent and the solid was collected. 1 M HCl was added to the solid until the solution had pH 1. The filtrate **(5)** was collected via vacuum filtration and washed with de-ionized water. (Yield = 86.97%.)

The fifth step added a third aramid with a Boc protecting group. Boc-4-aminobenzoic acid, EDCI, and DMAP were mixed with the previous product **(5)** (17.23 mmol) in DMF and mixed at room temperature overnight. The product **(6)** was crashed out in water, collected through vacuum filtration, and washed with MeOH. (Yield = 90.10%.)

The sixth removed the Boc protecting group from the amine end group. The previous product **(6)** (15.52 mmol) was dissolved in 1:9 solution of TFA and chloroform and stirred for 2 hours. Next, sodium bicarbonate was added and stirred for 2 hours. Vacuum was used to remove the solvent and TFA, and the product **(7)** was crashed out in water, collected through vacuum filtration, and washed with water. (Yield = 101.4%.)

The pathway described above optimizes the synthesis by leveraging repetitive steps and simpler purification compared to the original pathway proposed by Cho et al. [17]. By following this synthetic route, we were able to synthesize 15.35 mmol (6.8224 g) of the aramid structure **(7)** in one batch. This greater efficiency may enable

future automation of steps in the synthesis. Through a life cycle analysis (LCA), it was found that the aramid structure was produced at a cost of 16.48 dollars per gram.

## 2.3 Attachment of charged head groups

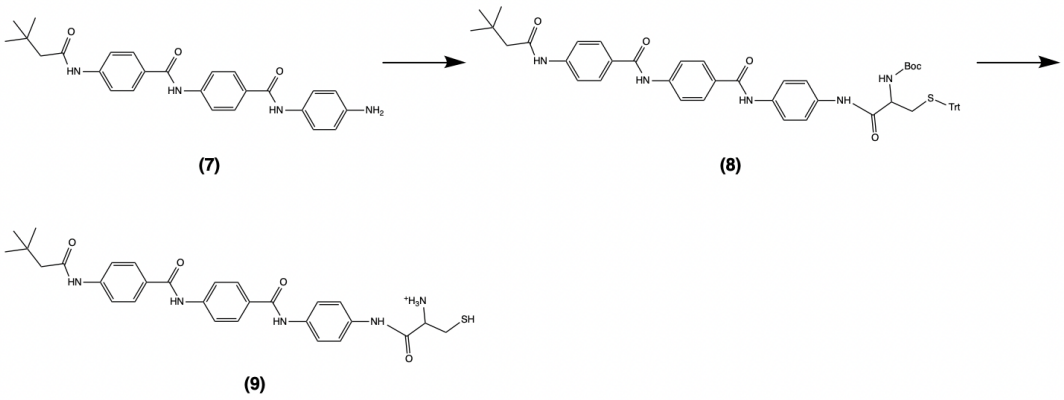


**Figure 2-2:** Synthetic route to attach the cysteine charged head group to the aramid structure.

There were two steps to functionalize with cysteine (Figure 2-2).

The first step was attach the head group to the amine group. Boc-Cys(Trt)-OH, EDCI, HOBt, and DIPEA were mixed with the previous product **(7)** (15.35 mmol) in a 1 to 1 ratio of DCM and DMF and left to stir at room temperature overnight. The next day, vacuum was used to remove excess solvent, the solid was crashed in water, and collected via vacuum filtration and dissolved with ACN to separate from impurities. The solid was separated via vacuum filtration and vacuum was used to remove excess solvent. DCM was added and the solution which was then sonicated before the product **(8)** was collected via vacuum filtration.

The second removed the Boc and Trt protecting groups from the amine end group. The previous product **(8)** (0.3416 mmol) was dissolved with TIPS in a 1:9 ratio of TFA and DCM and left to stir at room temperature overnight. The next day, DEE was added to the solution which was then sonicated before the product **(9)** was collected via vacuum filtration.

Additionally, a previously synthesized aramid amphiphile with positively charged

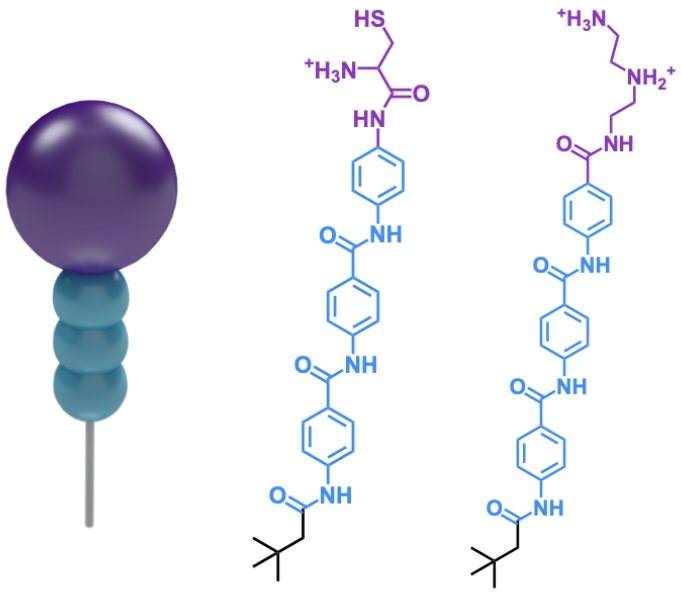


**Figure 2-3:** Schematic of an individual amphiphile (left) with chemical structure of CysAA (middle) and CatAA (right).

head group (cationic AA, or CatAA) was used as a control to compare against CysAA in terms of ability to bind to gold. The chemical structures of CysAA and CatAA are shown in Figure 2-3.

The self-assembled CysAA solution was prepared with a 1 mg solid to 1 mL water ratio, while the Cat AA was prepared with a 10 mg solid to 1 mL water ratio. We note that CysAA forms nanotube structures in water while CatAA forms nanoribbons.

# Chapter 3

# Supramolecular Gold Nanoparticle Catalysts

## 3.1 Gold nanoparticle affinity to CysAA

**Figure 3-1:** Prepared samples of AuNP-CysAA solutions in a 4 mL glass vial (left) and a 2 mL centrifuge tube (right).

A reactant-free solution of 10 nm colloidal gold in a stabilized suspension in 0.1 mM phosphate-buffered saline (Sigma Aldrich) was used in the catalysis demonstration experiments. 1 mL of gold solution was mixed with 100 uL of 1 mg/mL CysAA solution in a 2 mL centrifuge tube and left on a laboratory shaker for an hour to allow for AuNP binding onto CysAA (Figure 3-1). All preparations were carried out at room temperature.

An AuNP-CatAA solution was also prepared. The procedure was the same, except instead of CysAA, a 10 uL of 10 mg/mL CatAA solution was added.

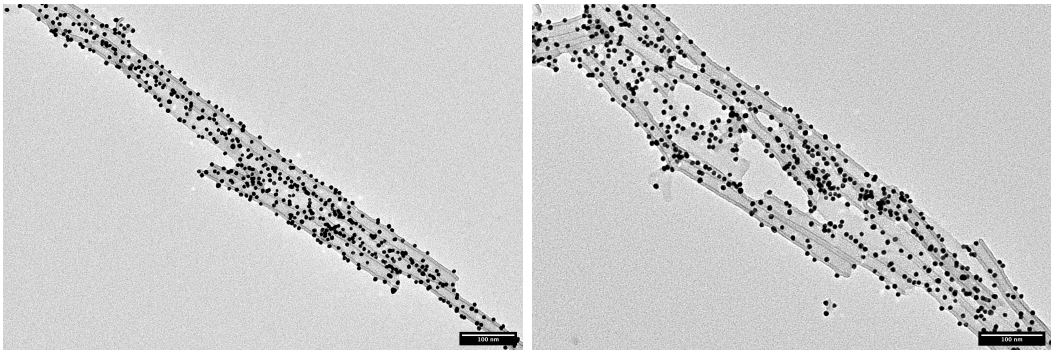

Images taken by Yukio Cho

**Figure 3-2:** TEM images of AuNPs binding evenly on the CysAA nanotubes.

Transmission electron microscopy (TEM) was used to verify that the AuNPs were binding to CysAA in the prepared solution. From the collected images, we observed AuNPs anchored evenly across the surface of CysAA nanotubes (Figure 3-2).

In contrast, TEM images of the AuNP-CatAA solution revealed random aggregation of AuNPs throughout the solution, without any correlation to the CatAA nanofibers (Figure 3-3). This behavior suggests that the AuNPs are bound securely via the gold-thiol bond to CysAA and not by the electrostatic interactions with the cationic head group of CatAA.

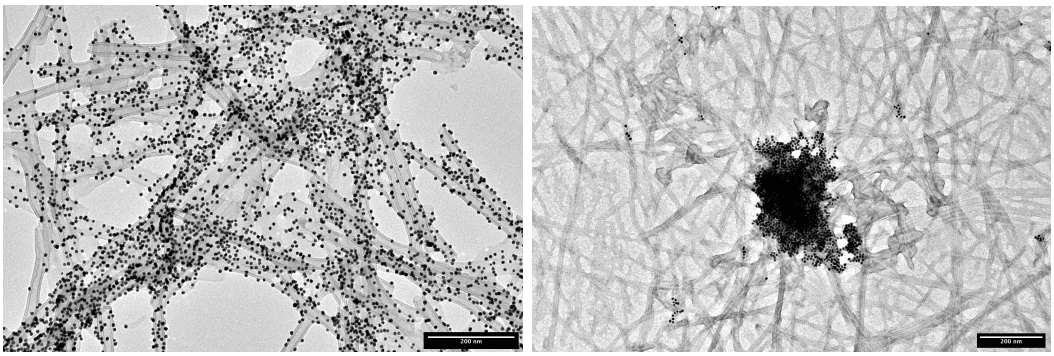

Images taken by Yukio Cho

**Figure 3-3:** TEM images of AuNP-CysAA vs. AuNP-CatAA showing AuNPs anchored evenly on CysAA and randomly aggregating in CatAA solution.

## 3.2 Catalytic evaluation of AuNPs via 4-nitrophenol reduction

In preparation for reaction, the AuNP-CysAA mixture was transferred to a 4 mL glass vial and 1 mL of de-ionized water was added, bringing the total volume of the catalyst solution to 2.1 mL (Figure 3-1). The concentration AuNPs in the final prepared sample was $2.85 * 10^{12}$ particles per mL.

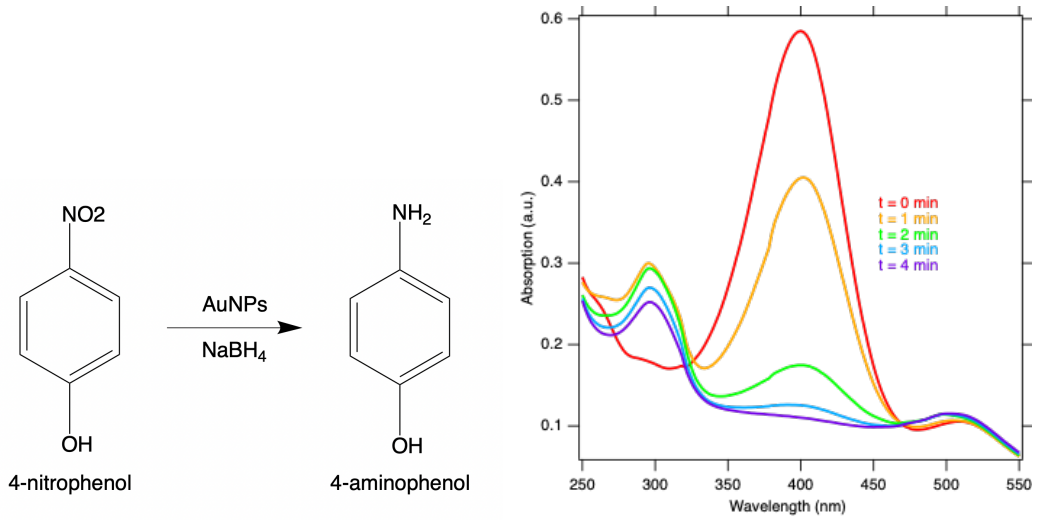


**Figure 3-4:** Reduction of 4-NP into 4-AP, used as a model reaction in this work (left). Multiple scans of UV absorption as the reduction of 4-NP progresses over a span of about 4 minutes (right). The decreasing peak at 400 nm corresponds to 4-NP while the increase peak at 300 nm corresponds to 4-AP.

The reduction of 4-nitrophenol (4-NP, Sigma Aldrich, ≥99%) into 4-aminophenol (4-AP) by sodium borohydride ($NaBH_4$, Sigma Aldrich, ≥96%) was used as a model reaction to demonstrate the catalytic activity of AuNPs tethered to our self-assembled molecular support (Figure 3-4). This reduction of 4-NP was chosen for the catalytic demonstration because of the clear shift in absorption peak as the reaction progresses (Figure 3-4). As such, by monitoring the reaction's absorption at 400 nm over time, the speed at which the reaction progresses can be deduced.

While the amount of each reagent was varied (discussed in next section) the final reactions were run with 50 uL of 1 mmol 4-NP and 50 uL of freshly prepared 50 mmol $NaBH_4$. Combined with the AuNP solution, there was a total volume of 2.2 mL.

Since the absorption peak shifts definitely as the reaction proceeds, we use Ultraviolet–visible spectroscopy (UV-vis) to track the progress of the reaction. The absorption at 400 nm was monitored over time, so that the kinetic profile of the reaction - and thus, the catalytic activity of the AuNPs - could be observed.

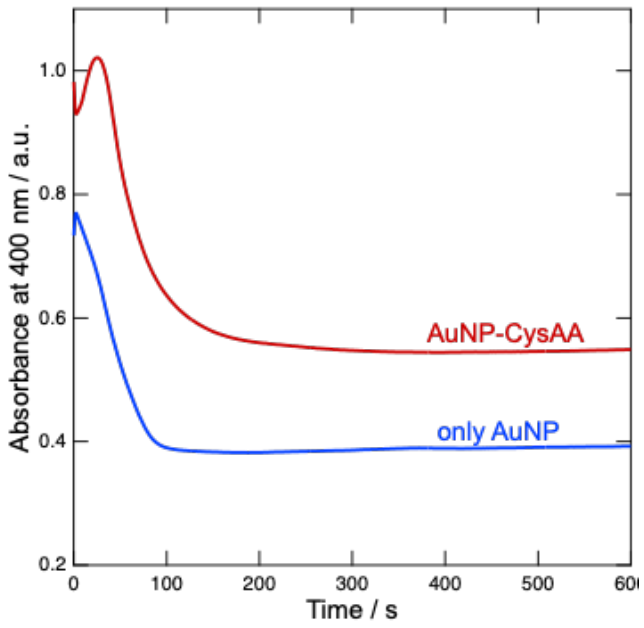


**Figure 3-5:** Kinetic profile of 4-NP reduction reaction catalyzed by colloidal AuNPs vs. AuNPs anchored on CysAA, gathered by monitoring the UV absorption at 400 nm over time. The peak of the S-curve corresponds to the start of the reaction while the onset of the tail regime corresponds to the end, when all 4-NP has been reduced.

In comparing kinetics of the reaction catalyzed by AuNP vs AuNP-CysAA, we found there to be a similar profile shape (Figure 3-5). There was a decrease in reaction time, which is to be expected from the introduction of any support material. The calculated rate constants were 0.015 $s^{-}1$ and 0.008 $s^{-}1$, respectively. We note that more trials are necessary to confidently quantify the kinetic performance of both scenarios, as the reaction rate may be influenced by slight experimental inconsistencies. However, it is clear that CysAA did not impede the AuNP's catalytic ability, a promising sign for its viability as a support material.

## 3.3 Recyclability of AuNP-CysAA catalysts

### 3.3.1 Filterability

The high aspect-ratio of CysAA nanotubes enables the recovery and reuse of AuNPs via simple filtration. Most syringe filters used had pore sizes in the range of 200 - 500 nm which would not be able to catch AuNPs of diameter $\leq$10 nm. However, the CysAA nanotubes have a median length of around 1 micron, which we hypothesize can be effectively trapped by the filter.

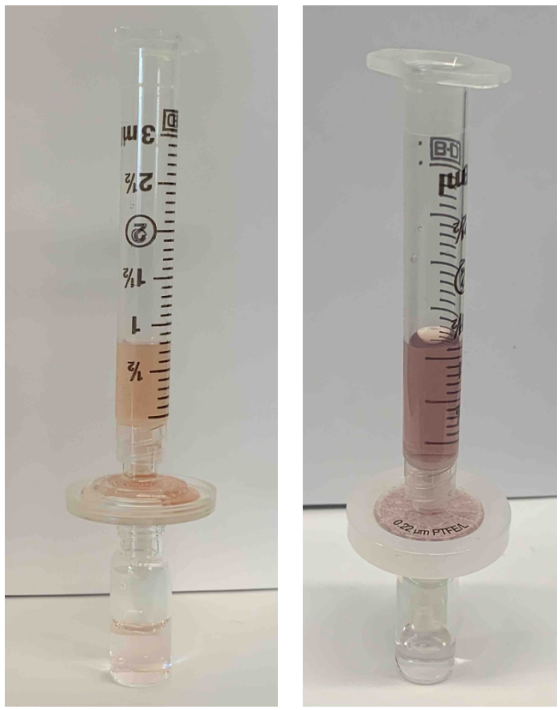

**Figure 3-6:** Syringe filter recovery of untreated AuNP solution (left) and of AuNP-CysAA solution (right). Critically, the AuNP solution was unable to be filtered and the filtrate is visibly pink compared to the clear AuNP-CysAA filtrate.

The AuNP-CysAA recovery was done using a syringe filter. The solution was simply left to sit and flow drop-wise through the filter, without pushing with the plunger of the syringe. The material, diameter, and pore size of the filters used were varied as experimental parameters (discussed in next section). Though not relevant to future reactions, the filtrate (liquid that passed through the filter) was recovered for analysis, specifically of gold or CysAA concentration, if any. The AuNP-CysAA

were recovered by drawing up 2.1 mL of de-ionized water through the syringe filter to achieve the same amount of AuNP per volume as the initial sample.

First, filtration of an untreated colloidal AuNP solution was attempted. We observed the pink clearly solution passing through the filter. Filtering an AuNP-CysAA solution, however, yielded a clear filtrate, indicating that AuNP was not passing through the filter in significant amounts (Figure 3-6).

**Figure 3-7:** Clear filtrate of repeated AuNP-CysAA recovery.

| Cycle Number | AuNP Concentration [ppm] |
|---|---|
| 1 | 0.01 |
| 2 | 0.03 |
| 3 | 0.02 |
| 4 | 0.03 |
| 5 | 0.51 |
| 6 | 0.03 |
| 7 | 0.01 |
| 8 | 0.01 |
| 9 | 0.01 |
| 10 | 0.01 |

Data collected by Ty Christoff-Tempesta

**Table 3.1:** Almost immeasurably low concentration of gold in the filtrate of repeated AuNP-CysAA recycling, via ICP analysis.

We then tried to extend the number of recovery cycles, where the recovered solution was collected and passed through the filter again. After ten cycles, the AuNP-CysAA showed no signs of passing through the filter (Figure 3-7). Inductively coupled plasma (ICP) spectroscopy was used to analyze the AuNP content of the filtrate. The

concentration was found to be 0.01 - 0.03 ppm, almost immeasurably low, indicating that AuNP-CysAA can effectively be filtered (Table 3.1).

### 3.3.2 Optimization of filter membrane and reagents

| Material | Diameter [mm] | Pore Size [um] | Good filter speed? | Separates AuNPs? | Doesn't stick to AuNPs? |
|---|---|---|---|---|---|
| PES | 25 | 0.45 | Yes | No | No |
| PES | 25 | 0.2 | Yes | Yes | No |
| PES | 13 | 0.2 | No | Yes | No |
| PVDF | 13 | 0.22 | No | No | No |
| PTFE | 13 | 0.22 | No | Yes | Yes |
| PTFE | 25 | 0.22 | Yes | Yes | Yes |

**Table 3.2:** Summary of filter optimization experiments.

Throughout experimentation, it was clear that minimizing AuNP loss throughout reaction cycles was the main challenge to sustaining catalytic performance. The syringe filter in particular emerged as an important component of the system that needed to be optimized to achieve consistent recycling (Table 3.2). We identified three key parameters of the filter: the pore size, diameter, and membrane material.

#### Reducing AuNP loss through the filter

Choosing an appropriate pore size for the filter was critical to minimizing gold loss. Simply put, a too-large pore size would allow AuNP-CysAA tubes to pass through, reducing the amount of gold available to catalyze the next cycle of reaction.

The two options considered were pores with diameter 0.45 um and 0.2 um. We were primarily considered with CysAA nanotubes that could pass through the pores length-wise; in other words, nanotubes that were shorter than the diameter of pore. A length distribution analysis was done using TEM images of synthesized CysAA and the image analysis software ImageJ, where the average and median lenghts were found to be 931 nm and 706 nm, respectively (Figure 3-8). From the sample represented in Figure 3-8, 30.3% of the nanotubes had lengths shorter than 0.45 um, whereas only 3.4% of the nanotubes had lengths shorter than 0.2 um. Thus, it is clearly evident

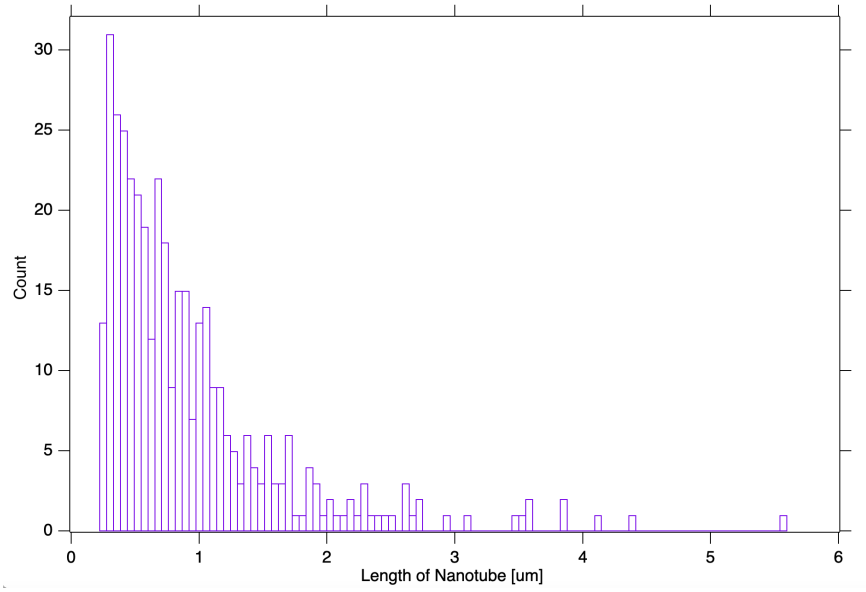


**Figure 3-8:** Length distribution of a sample of CysAA nanotubes.

how smaller pores prevent a significantly larger percent of CysAA tubes from passing through.

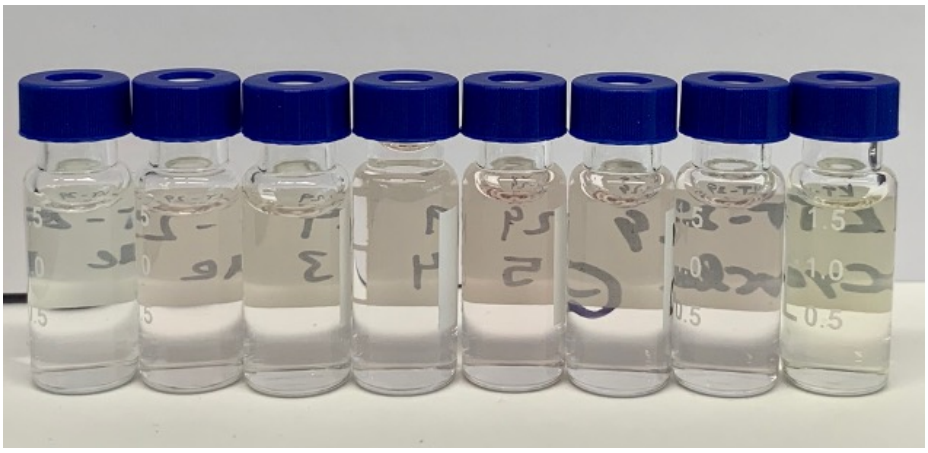

**Figure 3-9:** Filtrate of AuNP-CysAA recycling when used in reaction. The pink tint evident starting in the second cycle indicates AuNPs passing through the filter pores. (25 mm PES filter with 0.2 um pores.)

However, the issue of gold passing through the filter membrane was not completely solved by simply reducing the pore size. We observed that even with a 0.2 um pore size, at some point after the first cycle, the solution passing through the filter became pink - indicating the presence of AuNPs (Figure 3-9). To verify this observation, the solution was collected and flowed through multiple additional filters which produced

the same pink filtrate. This phenomenon indicated a fundamental problem with the recycling procedure: that either AuNPs were cleaving off of the CysAA support, or the CysAA nanotubes themselves were breaking and passing through the filter pores.

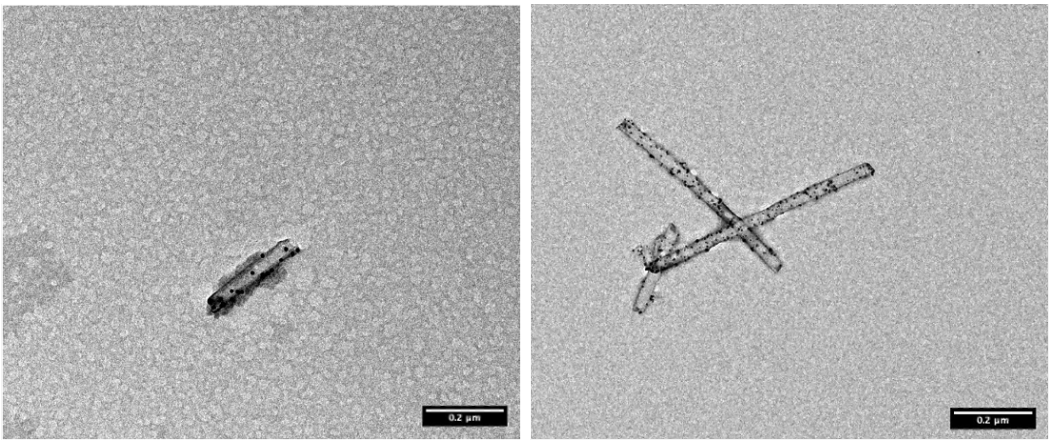


Images taken by Yukio Cho

**Figure 3-10:** TEM images of the pink-tinted solution that passed through the 25 mm PES 0.2 um pore filter showing broken CysAA tubes with AuNPs still attached.

TEM images of the filtrate revealed broken AuNP-CysAA tubes in the solution (Figure 3-10). We hypothesize that the cause of the CysAA nanotubes breaking was prolonged contact with excess $NaBH_4$, a powerful reducing agent.

To address this issue, we first decreased the concentration of $NaBH_4$ used in reaction, from 100 uL of 50 mM solution to 50 uL. We also tried a more drastic decrease to 20 uL. However, a decrease in reaction speed was observed from the first cycle, indicating that $NaBH_4$ had become to limiting reactant which obscures the AuNP catalyst effect on the kinetics of reaction.

Another measure we took was to reduce the total reaction time. While the first cycle (before any recycling) typically ran to completion in under 3 minutes, later cycles (usually starting from around the third cycle) took significantly longer, something up to 45 minutes. Following these prolonged reactions, we observed solution containing AuNP-CysAA flowing through the filter. To address this issue, we also decreased the amount of 4-NP (the reagent to be reduced), from 100 uL of 1 mM solution to 50 uL. This change allowed for the reaction to be consistently run under 10 minutes,

even later cycles as more AuNP was lost. More importantly, after these changes were made, we no long observed pink-colored filtrate passing through the filters during AuNP recovery.

| Cycle Number | AuNP Concentration [ppm] |
|---|---|
| 1 | 0.96 |
| 2 | 0.87 |
| 3 | 0.56 |
| 4 | 1.21 |
| 5 | 1.28 |
| 6 | 0.95 |
| 7 | 1.15 |
| 8 | 1.63 |
| 9 | 1.19 |
| 10 | 1.35 |

Data collected by Ty Christoff-Tempesta

**Table 3.3:** Low concentration of gold in the filtrate of repeated AuNP-CysAA recycling, via ICP analysis. (25 mm PTFE filter with 0.22 um pores.)

To confirm that AuNP was not being lost by passing through the filter, we again used ICP analysis on the filtrate with the 25 mm PTFE filter with 0.22 um pores, which revealed only trace amounts of AuNP in the solution, generally between 1 - 1.5 ppm.

### Reducing AuNP loss on the filter


**Figure 3-11:** 25 mm PES syringe filter (left) and 25 mm PTFE syringe filter (right). The PES is noticeably stained with AuNPs that stuck during recovery.

The other major source of gold loss was AuNP-CysAA sticking on the filter membrane. With the PES filter, the sticking was significant enough to be observed by the naked eye, as the membrane was stained pink after recycling (Figure 3-11).

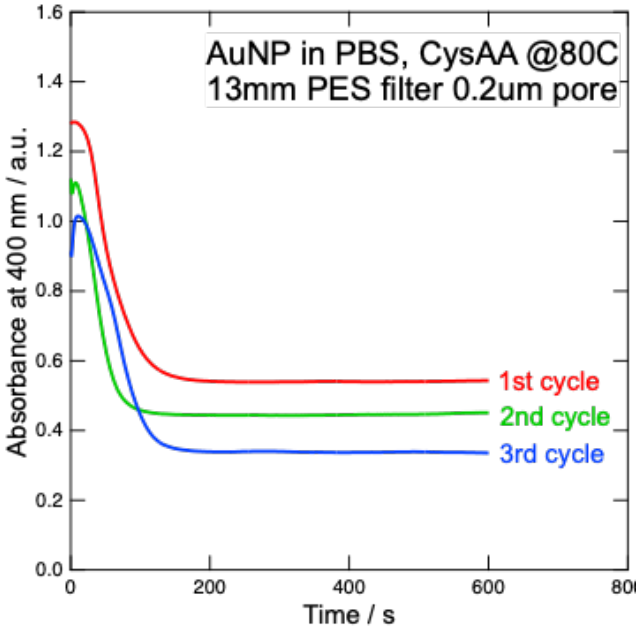


**Figure 3-12:** Kinetic profile of 3 cycles of 4-NP reduction catalyzed by the same AuNP-CysAA sample, recovered with a 13 mm PES filter with 0.2 um pores.

One strategy to mitigate AuNP-CysAA sticking to the filter was to simply reduce the surface area of the filter. To this end, we switched from a PES filter with 25 mm diameter to 13 mm. While there was still pink residue visible on the filter, the reduced AuNP loss was evident from the resulting absorption spectra. The second and third cycle displayed very similar spectra and reaction coefficient, indicating a consistent level of AuNP.

With the smaller filter diameter, however, the time for filtration was dramatically increased from about 20 minutes to over 90 minutes. Furthermore, it was difficult to recover solution up through the 13 mm syringe filter, which limited recycling to three cycles. While the increased AuNP recovery efficiency is certainly desirable, the practicality of the procedure is also an important consideration. Such low throughput makes the 13 mm syringe filter infeasible in industrial applications.

An alternative solution to reduce AuNP-CysAA sticking was to change the ma-

terial of the filter. The recycling procedure was tested with polyvinylidene fluoride (PVDF) and hydrophilic polytetrafluoroethylene (PTFE) membranes. None of the AuNP solution was able to pass through the PVDF filter, likely due to the hydrophobic nature of the membrane. The PTFE filter, however, proved to be the most effective at recovering the AuNP-CysAA. The filters were visibly clear of any pink residue, and the recovered gold was able to sustain more reactions cycles (Figure 3-11).

### 3.3.3 Demonstration of recycled catalysts

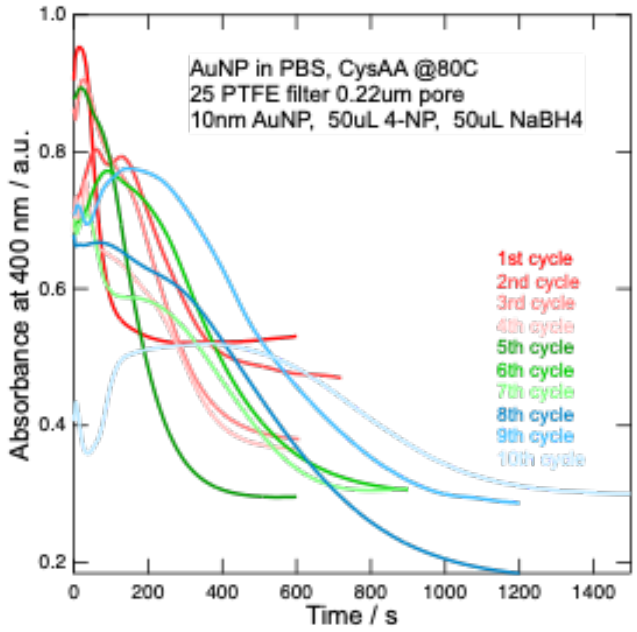


**Figure 3-13:** Kinetic profile of 10 cycles of 4-NP reduction catalyzed by the same AuNP-CysAA sample, recovered with a 25 mm PTFE filter with 0.22 um pores.

Using the 25 mm PTFE filter with 0.22 um sized pores, we were able to achieve up to 10 cycles of reuse with the same sample of AuNP-CysAA. While the reaction did get slower over cycles - likely due to small amounts of inevitable AuNP loss - we still observe the characteristic S-curve shape in the kinetic profile (Figure 3-13). The reaction was also able to consistently run to completion within 20 minutes.

We also note that the AuNP-CysAA platform does not degrade between cycles, with a timescale of at least a week. Cycles 1-4 (red), cycles 5-7 (green), and cycles 8-10 (blue) were collected on three different days over the course of a week. The

changes across the different days seem more dependent on the cycle number itself; in other words, there was no significant decrease in reaction rate observed after leaving the sample for several days.

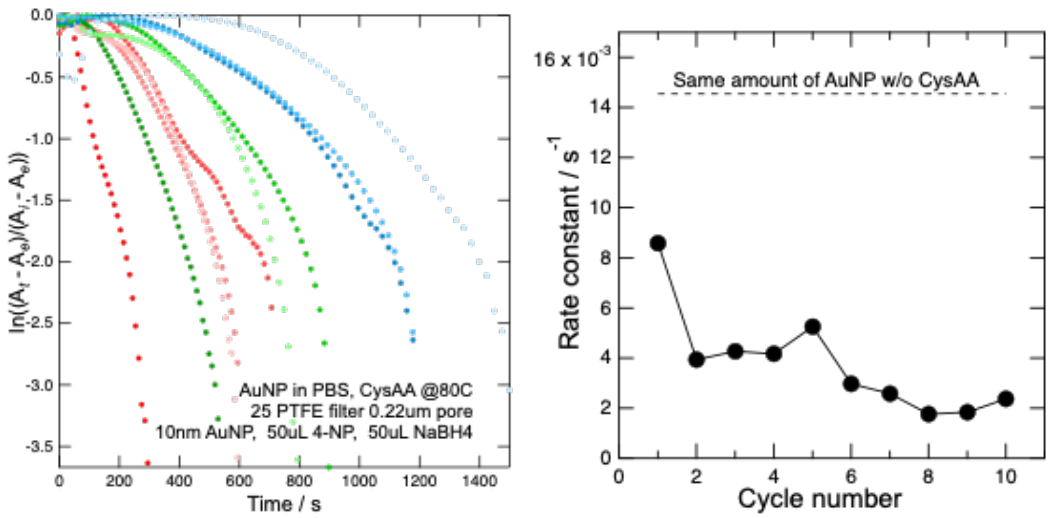


**Figure 3-14:** Normalized kinetic profile of the 10 reused cycles shown in Figure 3-13 (left). The slope of each curve gives the rate constant in each cycle (right).

We also plot the normalized kinetic profile of the 10 reused cycles (Figure 3-14). In this representation, the curve for each cycle is essentially non-dimensionalized by plotting the percent progress of the reaction with respect its own minimum and maximum absorbance against time. By doing so, we can gain insight into the reaction kinetics without influence from the different baseline values across cycles, which can be shifted by different concentrations of gold. One such insight is the rate constant, which is represented as the slope of the curve. Plotting the rate constant against cycle number reveals an initial drop from the first cycle (before any recycling) and a relatively stable rate afterwards (Figure 3-14). While the AuNP-CysAA is likely nearing the end of its utility by the 10th cycle, its recyclability is already an improvement over conventional homogeneous catalysis, where recycling is difficult or impossible.

To quantify the activity of the catalyst, we calculate both the turnover number (TON) and turnover frequency (TOF) of the AuNP-CysAA catalyst in the first and last cycle. The TON represents the amount of reagent that can be converted per unit catalyst, and is given by the expression

$$TON = n_{product}/n_{catalyst} \tag{3.1}$$

where $n$ is the number of moles. Given a conservative estimate that only 80% of the 4-NP is converted to 4-AP and that there is the same amount of gold throughout all ten cycles, it can be calculated that the $TON = 4026.76$.

TOF represents the amount of reagent converted per unit time, and is frequently used to compare catalytic activity across systems. We can simply divide by the reaction time for each cycle to obtain

$$TOF_{cyc1} = 21.5s^{-1}$$
$$TOF_{cyc10} = 6.0s^{-1}$$

which falls in the range for most industrially applicable catalysts [19].

# Chapter 4

# Conclusions and Future Work

This work serves as preliminary proof of concept for a self-assembled platform for gold nanoparticle catalyst stabilization. We present a novel support material, the cysteine-functionalized aramid amphiphile (CysAA) that self-assembles into stable nanotubes in water. CysAA is designed to have chemical affinity to gold and high surface area to anchor AuNPs. Additionally, its mechanical robustness and high aspect-ratio enables recovery and reuse of the AuNP-CysAA catalyst, which is promising for potential industrial applications.

The most immediately relevant future work is to explore the viability of different sized gold nanoparticles with the CysAA platform. This work only investigated 10 nm AuNPs; colloidal gold with smaller diameters such as 5, 3, and even 1.8 nm are commercially available and could be tested.

Further analysis can be done to quantitatively characterize the bond between the AuNPs and CysAA. Analytical techniques such as X-ray photoelectron spectroscopy (XPS) or Fourier Transform Infrared Spectroscopy (FTIR) can be employed to do so.

This research could also be expanded to different metal nanoparticle catalysts, such as silver or platinum nanoparticles, either directly using CysAA or using an AA platform with a different head group.

# Bibliography


[1] Ibrahim Khan, Khalid Saeed, and Idrees Khan. Nanoparticles: Properties, applications and toxicities. *Arabian journal of chemistry*, 12(7):908–931, 2019.

[2] Monic Shah, Vivek D Badwaik, and Rajalingam Dakshinamurthy. Biological applications of gold nanoparticles. *Journal of Nanoscience and Nanotechnology*, 14(1):344–362, 2014.

[3] A Sanchez, S Abbet, U Heiz, W-D Schneider, H Häkkinen, RN Barnett, and Uzi Landman. When gold is not noble: nanoscale gold catalysts. *The Journal of Physical Chemistry A*, 103(48):9573–9578, 1999.

[4] David T Thompson. Using gold nanoparticles for catalysis. *Nano Today*, 2(4):40–43, 2007.

[5] Saji Alex and Ashutosh Tiwari. Functionalized gold nanoparticles: synthesis, properties and applications—a review. *Journal of nanoscience and nanotechnology*, 15(3):1869–1894, 2015.

[6] Xue Bai, Yueying Wang, Zhiyun Song, Yanmin Feng, Yuanyuan Chen, Deyuan Zhang, and Lin Feng. The basic properties of gold nanoparticles and their applications in tumor diagnosis and treatment. *International journal of molecular sciences*, 21(7):2480, 2020.

[7] Sónia AC Carabineiro. Supported gold nanoparticles as catalysts for the oxidation of alcohols and alkanes. *Frontiers in Chemistry*, page 702, 2019.

[8] Zhen Ma and Sheng Dai. Development of novel supported gold catalysts: A materials perspective. *Nano Research*, 4(1):3–32, 2011.

[9] Thiemo A Faßbach, Robin Kirchmann, Arno Behr, and Andreas J Vorholt. Recycling of homogeneous catalysts in reactive ionic liquid–solvent-free aminofunctionalizations of alkenes. *Green Chemistry*, 19(21):5243–5249, 2017.

[10] Ramón Pamies, José Ginés Hernández Cifre, Vanesa Fernández Espín, Mar Collado-González, Francisco Guillermo Díaz Baños, and José García de la Torre. Aggregation behaviour of gold nanoparticles in saline aqueous media. *Journal of nanoparticle research*, 16(4):1–11, 2014.

[11] Eric M Gaigneaux, DE De Vos, PA Jacobs, JA Martens, P Ruiz, G Poncelet, and P Grange. *Scientific bases for the preparation of heterogeneous catalysts*. Elsevier, 2002.

[12] Graham J Hutchings. Heterogeneous gold catalysis. *ACS central science*, 4(9):1095–1101, 2018.

[13] Xiaochun Zhou, Weilin Xu, Guokun Liu, Debashis Panda, and Peng Chen. Size-dependent catalytic activity and dynamics of gold nanoparticles at the single-molecule level. *Journal of the American Chemical Society*, 132(1):138–146, 2010.

[14] David Chandler. Interfaces and the driving force of hydrophobic assembly. *Nature*, 437(7059):640–647, 2005.

[15] George M Whitesides, John P Mathias, and Christopher T Seto. Molecular self-assembly and nanochemistry: a chemical strategy for the synthesis of nanostructures. *Science*, 254(5036):1312–1319, 1991.

[16] Ty Christoff-Tempesta, Yukio Cho, Dae-Yoon Kim, Michela Geri, Guillaume Lamour, Andrew J Lew, Xiaobing Zuo, William R Lindemann, and Julia H Ortony. Self-assembly of aramid amphiphiles into ultra-stable nanoribbons and aligned nanoribbon threads. *Nature Nanotechnology*, 16(4):447–454, 2021.

[17] Yukio Cho, Ty Christoff-Tempesta, Dae-Yoon Kim, Guillaume Lamour, and Julia H Ortony. Domain-selective thermal decomposition within supramolecular nanoribbons. *Nature communications*, 12(1):1–7, 2021.

[18] Thomas Bürgi. Properties of the gold–sulphur interface: from self-assembled monolayers to clusters. *Nanoscale*, 7(38):15553–15567, 2015.

[19] Robert Roskoski. Michaelis-menten kinetics. In *Reference Module in Biomedical Sciences*. Elsevier, 2015.